Available online at www.sciencedirect.com
SCIENCE DIRECT®
ELSEVIER
ISPRS Journal of Photogrammetry & Remote Sensing 1267 (2003) 1–12
PHOTOGRAMMETRY & REMOTE SENSING
www.elsevier.com/locate/isprsjprs

Detection of building outlines based on the fusion of SAR and optical features

F. Tupin*, M. Roux

ENST, Dept. TSI, CNRS URA 820, 46 rue Barrault, 75634 Paris Cedex 13, France

Received 28 June 2002; accepted 31 January 2003

Abstract

This paper deals with the automatic extraction of building outlines using a pair of optical and synthetic aperture radar (SAR) images. The aim is to define areas of interest for building height reconstruction in radargrammetric or interferometric applications. Since high resolution optical satellite images are now easily available, such methods merging SAR and optical information could be useful to improve 3D SAR reconstruction (the optical image giving only information on the scene organization). Both SAR and optical data bring complementary information about the building presence and shape. The proposed method is divided into two main steps: first, extraction of partial potential building footprints on the SAR image, and then shape detection on the optical one using the previously extracted primitives (lines). Two methods of shape detection have been developed, the simplest one finding the "best" rectangular shape and the second one searching for a more complicated shape in case of failure of the first one. Results for an industrial area acquired with two incidence angles for the SAR image are presented and analyzed.

Keywords: building detection; SAR images; optical images; edge extraction; fusion

1. Introduction

There are at present many synthetic aperture radar (SAR) sensors providing a wide area coverage of the planet (either satellite sensors like ERS-2, RadarSat, EnviSat and shuttle missions (Jordan, 1997), or even aerial acquisitions (Gamba et al., 2000)) due to the full-time imaging potential of radar.

Computation of digital elevation models with SAR data (either in radargrammetric (Simonetto et al., 2001) or interferometric (Bolter and Leberl, 2000; Gamba et al., 2000) applications) in urban areas is still difficult and often provides insufficient results. The introduction of a pre-processing step of scene analysis giving the image organization could be useful to improve the height reconstruction step. But interpretation of SAR images in urban or semi-urban areas remains particularly difficult due to the geometric perturbations (lay-overs, shadows) and to the speckle noise. On one hand, in many cases, the building shapes are hardly recognizable in the SAR data depending on the wavelength and incidence angle.

* Corresponding author. Tel.: +33-1-45-81-72-45; fax: +33-1-45-81-37-94.
E-mail address: tupin@tsi.enst.fr (F. Tupin).

0924-2716/03/$ - see front matter © 2003 Published by Elsevier Science B.V.
doi:10.1016/S0924-2716(03)00018-2

Although some attempts have been made to directly extract the building shapes on one SAR image (Simonetto et al., 2001), results are often incomplete. On the other hand, some parts of the building are easily seen on the radar data, thus providing useful information about their potential localization. High resolution optical satellite images are now easily available. It could be interesting to use them to detect potential building areas and thus help the 3D reconstruction of the SAR data (either in radargrammetric or interferometric applications). The optical images are of course much more easier to interpret and many methods for automatic building detection on monocular images have been developed (Shufelt and McKeown, 1993; Jaynes et al., 1994; Lin et al., 1995; Shufelt, 1999). Nevertheless, good results are mostly obtained in the case of stereovision applications using both elevation data and two optical images in the detection step (Oriot et al., 1998; Hanson et al., 1997).

Since both SAR and optical images bring information for building detection, it is interesting to use both of them in the context previously exposed. The aim of this paper is therefore to study how SAR and optical images could be simultaneously used for building detection purposes. The general framework of this study was radargrammetric applications and the building detection was a preliminary step to the height reconstruction one (Tupin, 2002). This context is thus rather different from other work on fusion between optical and radar data. Indeed, most of them present classification methods (Hellwich et al., 2000; Fatone et al., 2001; Xiao et al., 1998b), whereas this article is dedicated to shape recognition by fusion of SAR and optical features. Besides, no height information is used in the developed approach (contrary to Xiao et al., 1998a, for instance with interferometric data).

2. Overview of the proposed method

Fig. 1 presents a small part of a SAR image and the corresponding optical image. The optical image has been acquired by the camera of the French National Geographical Institute (IGN) and the resolution is 50 cm. The SAR images have been generated by the S-band of the RAMSES sensor of the French DGA (Defense Procurement Agency) with an approximate resolution of 50 cm.

As said before, without external knowledge, the SAR image interpretation is quite difficult, even for a human photo-interpreter. Nevertheless, very bright lines appear along the surface discontinuity formed by the building and the ground due to the double bounce reflections along the building wall, as described in Simonetto et al. (2000). This is the case

Fig. 1. Examples of the building appearance in the slant range SAR image with sensor viewing from the left (left) and the corresponding optical image (right).

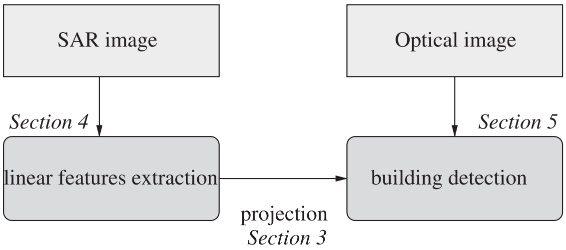

Fig. 2. Synopsis of the proposed building detection method.

for the building part oriented towards the sensor, whereas the other parts are not clearly seen in the image. Besides, since the S-band wavelength is rather long compared to the roughness of man-made objects, reflections of the roofs are hardly visible (depending on the roof material). The SAR data can therefore be used to focus attention on specific areas in the optical image to do the building shape extraction. Besides, the probable orientation and sometimes the length of a building side is given by the SAR data, since it corresponds to the length and orientation of the corresponding bright linear feature. We propose to use this information to constrain the building shape search in the optical image.

The article is divided in three main parts. The first part recalls some principles of the SAR and optical acquisition systems and presents the way to project points between each other. The second part is dedicated to the processing of the SAR image, specially the bright linear feature extraction. The third part presents the method developed for building detection in the optical image, constrained by the detected SAR lines. Results on real SAR and optical images will be presented in this part and the limits and possible improvements of the method will be underlined. Fig. 2 presents the synopsis of the method and the corresponding sections.

3. Optical and SAR acquisition systems and point projections

To project points from optical to SAR data and conversely we need some transformation functions. They are based on the computation of the 3D coordinates of the point and on the knowledge of the sensor acquisition system parameters.

3.1. SAR equation

The principle of the SAR system is based on the emission of electromagnetic waves, which are then backscattered by the surface elements. For a given time of acquisition t, the imaged points lie in the intersection of a sphere of range $R = ct$ and a cone related to the pointing direction of the antenna. More precisely, let us denote by S the sensor position, by $\overrightarrow{V}$ the speed of the sensor and by θ_D the Doppler angle, which is related to the Doppler frequency f_D and the speed by $\cos(\theta_D) = \lambda f_D / 2|\overrightarrow{V}|$; then, the SAR equations for an object point M are given by:

$$SM^2 = R^2 \tag{1}$$

$$R\sin(\theta_D)V = \overrightarrow{SM} \cdot \overrightarrow{V} \tag{2}$$

Knowing the line i and column j of a pixel and making a height hypothesis h, the 3D coordinates of the corresponding point M are recovered using the previous equations. R is given by the column number j, the resolution step δ and the near range R_o, by $R = j \times \delta R + R_o$. Thus, the 3D point M is the intersection of a sphere with radius R, the Doppler cone of angle θ_D and a plane with altitude h. The coordinates are given as solutions of a system with three equations and two unknowns (since the height must be given).

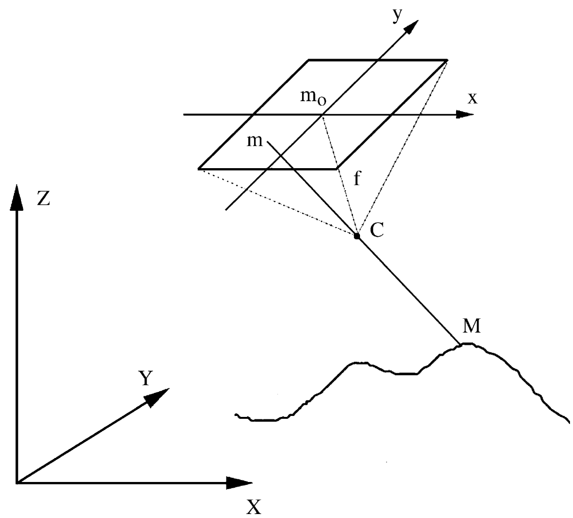

Fig. 3. Image acquisition geometry of the optical system.

Conversely, knowing the 3D point M, the (i, j) pixel image coordinates can be recovered by computing the sensor position for the corresponding Doppler angle (which provides the line number) and then deducing the sensor-point distance, which permits the definition of the column number, since $j = (R - R_o)/\delta R$.

3.2. Optical acquisition system

The geometrical model for optical image acquisition is completely different and is based on the collinearity equations. Each point of the image is obtained by the intersection of the image plane and the line joining the 3D point M and the optical center C (see Fig. 3). The equation system between the image coordinates (x_m, y_m) and the 3D point M (X_M, Y_M, Z_M) is given by:

$$x_m = \frac{a_{11}X_M + a_{12}Y_M + a_{13}Z_M + a_{14}}{a_{31}X_M + a_{32}Y_M + a_{33}Z_M + a_{34}} \tag{3}$$

$$y_m = \frac{a_{21}X_M + a_{22}Y_M + a_{23}Z_M + a_{24}}{a_{31}X_M + a_{32}Y_M + a_{33}Z_M + a_{34}} \tag{4}$$

where the a_{ij} coefficients are some system parameters. Once again, a height hypothesis is necessary to define M from (x_m, y_m).

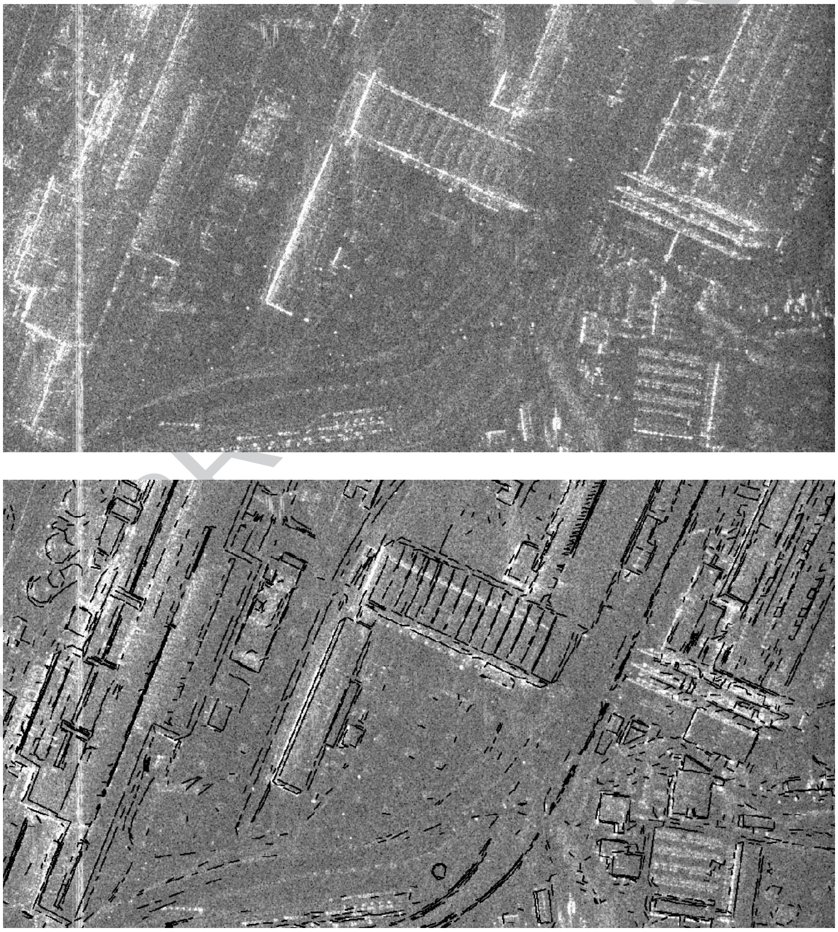

Fig. 4. Slant range SAR image (top) and the super-imposition of the contours detected on the optical image (bottom).

3.3. SAR to optical image projection and conversely

The co-registration of the SAR and optical image require the perfect knowledge of the acquisition parameters. Knowing them, the projection is made using an intermediate 3D point.

An example of the projection of features extracted in the optical image is presented in Fig. 4. The features are edges extracted by the Canny–Deriche detector (Canny, 1986) in the optical image. They are then projected in the SAR geometry using the ground height as height hypothesis (8 m here). This is the reason why the ground features of the SAR data seem well matched, whereas the edges above the ground (roof responses) are displaced compared to the SAR responses.

Nevertheless, such a projection is of great help to understand SAR backscattering mechanisms and help the definition of adapted tools.

4. Processing of the SAR image

As explained before, the edges of buildings oriented towards the sensor usually appear as bright lines in the SAR image. A line detector is thus used to extract such features related to the building presence.

4.1. Line detector

The line detector has previously been proposed in Tupin et al. (1998). It is based on the fusion of the results from two line detectors D1 and D2, both taking the statistical properties of speckle into account. Both detectors have a constant false-alarm rate (that is, the rate of false alarms is independent of the average radiometry of the considered region, as defined in Touzi et al., 1988). Line detector D1 is based on the ratio edge detector (Touzi et al., 1988), widely used in coherent imagery. Detector D2 uses the normalized centered correlation between two populations of pixels. Both responses from D1 and D2 are merged in order to obtain a unique response as well as an associated direction in each pixel. The detection results are post-processed to provide candidate line segments.

We just recall here the line detector expressions (a detailed study can be found in Tupin et al., 1998). The response of the ratio edge detector between two regions i and j of radiometric means μ_i and μ_j is defined as r_{ij}:

$$r_{ij} = 1 - \min\left(\frac{\mu_i}{\mu_j}, \frac{\mu_j}{\mu_i}\right) \tag{5}$$

and the response to D1 as $r = \min(r_{12}, r_{23})$, the minimum response of a ratio edge detector on both sides (with indexes 1 and 3) of the linear structure (with index 2).

The cross-correlation coefficient ρ_{ij} between two regions i and j can be shown to be:

$$\rho_{ij}^2 = \frac{1}{1 + (n_i + n_j)\dfrac{n_i \gamma_i^2 \overline{c_{ij}}^2 + n_j \gamma_j^2}{n_i n_j (\overline{c_{ij}} - 1)^2}} \tag{6}$$

where n_i is the pixel number in region i and $\overline{c_{ij}} = \mu_i/\mu_j$ is the empirical contrast between regions i and j, and γ_i the variation coefficient (ratio of standard deviation and mean), which adequately measures homogeneity in radar imagery scenes. This expression depends on the contrast between regions i and j, but also takes into account the homogeneity of each region, thus being more coherent than the ratio detector (which may be influenced by isolated values). In the case of a homogeneous window $\mu_i = \mu_j$, ρ_{ij} equals 0 as expected. As for D1, the line detector D2 is defined by the minimum response ρ of the filter on both sides of the line: $\rho = \min(\rho_{12}, \rho_{23})$.

Then, both responses are merged using an associative symmetrical sum $\sigma(x, y)$, as defined in Bloch (1996):

$$\sigma(x, y) = \frac{xy}{1 - x - y + 2xy} \quad \text{with } x, y \in [0, 1] \tag{7}$$

A theoretical and simulation based study could be used to define the threshold level depending on a false alarm and a detection rate. In fact, due to the unknown distribution of the bright pixels along the building/ground discontinuity, such a study is difficult and in this case the detection threshold has been empirically chosen.

4.2. Application and results

The line detection process is applied on a reduced image. Size reduction is done by 2×2 block averaging. Indeed, the searched lines are quite thick on the one hand and not very homogeneous on the other hand. Some points along the line have a higher radiometric value than the other ones, thus disturbing the detection process. These problems are overcome by the averaging which reduces the speckle effect, and makes lines more homogeneous.

In a radargrammetric framework, the linear features can be filtered depending on their direction and their relative position in both SAR images of the stereopair (only matched lines with low height are then kept). A result of the line detection is presented in Fig. 5. Most of the brightest lines have been extracted, with some false alarms due to isolated bright points.

5. Constrained building detection in the optical image

After detection, the SAR lines are then projected on the optical imagery using a height hypothesis for the ground height (here a flat ground of 8 m is assumed). Only the extremities of the line are projected and a straight line approximation is made (this is not exact but since the lines are quite short, this approximation gives acceptable results). Some

Fig. 5. Detection of the brightest linear features (black lines) in the SAR data.

results are presented in Fig. 6. In the following, a SAR primitive is a projected line segment representing the side of a potential building. The aim of this section is to associate to each SAR primitive a building shape with a confidence level, allowing the suppression of the false alarms of the previous step.

The detection difficulty is related to many parameters: shape complexity of the building, contrast between the building and the background, presence of structures on the roof.

5.1. Method principle

Two approaches have been developed. The first one is faster but provides only rectangular shapes and the second one is slower but is able to detect more complicated shapes.

Both of them are applied on a set of edges extracted from the optical image by the following steps:

- Application of the Canny–Deriche edge detector (Canny, 1986);

Fig. 6. Examples of projection of the SAR primitives (white lines) to the optical image.

- Thinning of the edges (Deutsch, 1972);
- Polygonal approximation of the edges to obtain a vectorial representation.

A filtering of the optical edges is also applied based on proximity and direction criteria:

- Firstly, for each SAR primitive, an interest area is computed using the sensor viewing direction as indicated in Fig. 7;
- Secondly, only the edges, which are parallel or perpendicular to the SAR primitive, are selected (with an angular tolerance).

Both the set of filtered edges and the Canny–Deriche response image will be used in the following.

5.1.1. Best rectangular shape detection

First, the building side is detected and then an exhaustive box search is done.

The building side is defined as the parallel optical edge $\vec{s_o}$, which is close to the SAR primitive and has the higher mean of the edge detector responses. Since the extremities of the edge (denoted by M_o^1 and M_o^2 may be not exactly positioned, a new detection is applied along the previously detected edge $\vec{s_o}$. Three candidate extremities are kept for each extremity. To do so, a search area of length s_1 is defined around M_o^i (Fig. 8) and each point M in this area is attributed a score depending on the edge detector responses along a small segment $\vec{s_o^p}(M)$ perpendicular to $\vec{s_o}$. The three points with the best scores are kept for each M_o^i. They are denoted by $M_o^i(p)$, with $1 \le p \le 3$.

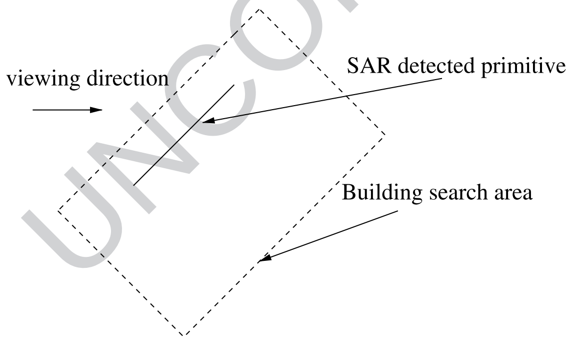

Fig. 7. Definition of the search area for each detected SAR primitive.

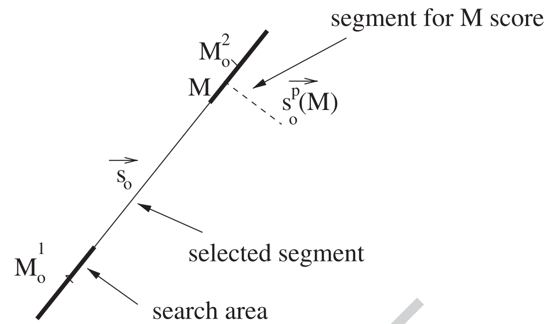

Fig. 8. Selection of new extremity candidates (the search area corresponds to the bold segment at each extremity M_o^i).

The rectangular box detection is then applied for each possible pair of extremities $(M_o^1(p), M_o^2(q))$, with $1 \le p \le 3$ and $1 \le q \le 3$. For each pair, a rectangular box of variable width w is defined and an associated score is computed. For each side k of the box ($k=1$, 2), the mean $\mu(k)$ of edge detector responses along the box side is computed. Then, the score of the box $S(M_o^1(p), M_o^2(q), w)$ is defined by:

$$S(M_o^1(p), M_o^2(q), w) = \min_k \mu(k) \quad (8)$$

This fusion method, based on the minimum response, gives a weak score to boxes, which have a side that does not correspond to an edge. For each extremity pair $(M_o^1(p), M_o^2(q))$, the width w is varied and the one giving the highest score is selected. The final box is the one with the highest score among all possible extremity pairs and it is selected for further processing, if its score is higher than the threshold th_1. Some results are presented in Fig. 9.

This method gives quite good results for rectangular buildings and for SAR primitives with good position and size.

5.1.2. Complex shape detection

In the case of more complicated shapes, a different approach should be used. We adopted the strategy similar to the one of Roux and McKeown (1994), which is based on the detection of specific features. Here, we decided to focus on corners and to define a building as a set of joined corners.

Fig. 9. Results of the best rectangular box detection. The three circles at the end regions of each left edge of the buildings correspond to the candidate extremities, which have been detected. The SAR primitive and the best box (building outline) are also shown.

First of all, a set of candidate corners is detected using the optical filtered edges. For each edge, two corners are detected. As in the previous section, a search area of length s_2 is centered at each extremity and the corner with the best score is selected. A corner is defined as two intersecting edges (not necessarily orthogonal to each other), the score of an edge is defined as the mean of the edge detector responses (as previously) and the corner score as the minimum score along the two edges. The corners are filtered and only the corners with a score above a threshold thc_2 are selected.

Secondly, a starting edge $\vec{s_0}$ is detected in the same way as before. Starting from this edge, a search area is defined as previously but with a much bigger size s_g, since the building shape can be quite complicated. In this case, the SAR primitive is often only a small part of the building.

Starting from $\vec{s_0}$ and its corners, a path joining a set of corners is searched. To do so, a search tree is built starting from a corner. Let us denote by $(M_i, \vec{s_i}, \vec{t_i})$ a corner i ($\vec{s_i}$ and $\vec{t_i}$ are the two short edges defining the corner). The set of prolonging edges of corner i is then detected. A corner j is said to potentially prolong the corner i if the following conditions are fulfilled:

- The projection of M_j on the line $(M_i, \vec{t_i})$ is close to M_i;
- $\vec{s_j}$ or $\vec{t_j}$ is parallel and with an opposite direction compared to $\vec{s_i}$—we will denote by $\vec{u_j}$ the concerned vector in the following;

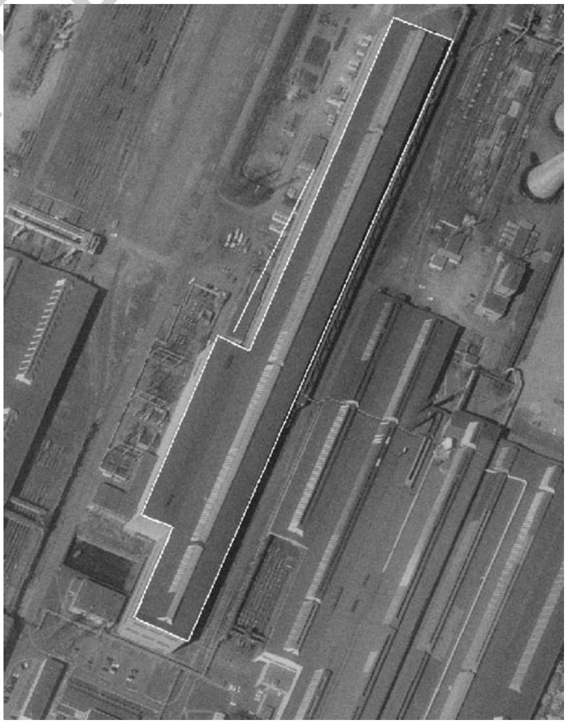

Fig. 10. Example of building detection (white polygon) using the corner search tree (the SAR primitive is also shown as a white line).

- Denoting $M_i' = M_i + \overrightarrow{s_i}$ and $M_j' = M_j + \overrightarrow{u_j}$, then $\overrightarrow{M_iM_i'} * \overrightarrow{M_jM_j}\mathrm{V} < 0$.

with * the dot product.

In the search tree, all the corner candidates are sons of i and the tree is iteratively built. A branch stops when a maximum number of levels is reached or when the reached node corresponds to the root. In the last case, a path joining the corners has been detected. All the possible paths in the search tree are computed and a score is attributed. Once again, the path score corresponds to the score minimum of the edges joining the corners. The best path gives the searched building shape and is validated, if it is higher than the threshold th_2. An example is given in Fig. 10.

6. Method evaluation

This section presents the results obtained on two SAR images and the corresponding optical image. First, the parameters involved in the method are enumerated and their influence is analyzed and then a quantitative and qualitative analysis of the results is given.

6.1. Involved parameters

Concerning the first step of SAR primitive detection, there is only one parameter which is the threshold th_l on the line detector. As usual, this threshold must be chosen to obtain a compromise between the false alarms and the non-detections. Since the false alarms (i.e. primitives which do not correspond to a building) can be suppressed by the subsequent step in the optical image, a choice minimizing the non-detections is preferable, although it increases the computing time, since more building detections will be launched.

Concerning the building detection by a rectangular box, the following parameters have to be set:

- The length s_1 of the search area for the extremity candidates of the box; this length should not be too large, since it increases the wrong detections; it is defined as a percentage of the length of the considered edge;
- The final threshold th_1 of the box score; once again, a compromise between false alarms (boxes which do not correspond to a building) and the non-detections must be made; since the second method is launched in case of failure of the first one, a choice minimizing the false alarm rate is preferable.

Concerning the building detection by complex shape, the following parameters have to be set:

- The length s_2 of the search area of the corners of an edge; it is defined as a percentage of the length of the considered edge;
- The threshold thc_2 of the corner score;
- The size s_g of the global area in which the building is searched; this size is also a percentage of the edge length;
- The depth of the corner tree; it is only limited to reduce the computing time;
- The final threshold th_2 on the detected shape; this time, the final results are related on it.

Instead of thresholding the detected shapes (th_1 and th_2), the scores could be used to define a confidence level associated to the detected building.

6.2. Result analysis

The results have been obtained with the following parameter set: $s_1 = 160\%$ of the considered edge, $\mathrm{th}_1 = 140$ (on the Canny–Deriche responses stretched on a 255 dynamic between the minimum and maximum values), $s_2 = 160\%$, $s_g = 500\%$, $\mathrm{th}_2 = 130$. Fig. 11 shows the super-imposition of the buildings detected by the two approaches. The fusion method is based on a hierarchical application of the two proposed methods. In case of failure of the rectangular box detection method (score below th_1), a corner search tree based method is launched. If the final score is high enough (above th_2), the building is kept.

The method has been applied on two SAR images of the same area but acquired with different incident angles (30° and 40°). Unfortunately, these angles are too close to give different results and the set of SAR primitives detected on both SAR images is very similar. Therefore, no conclusion about the influence of the incidence angle can be deduced.

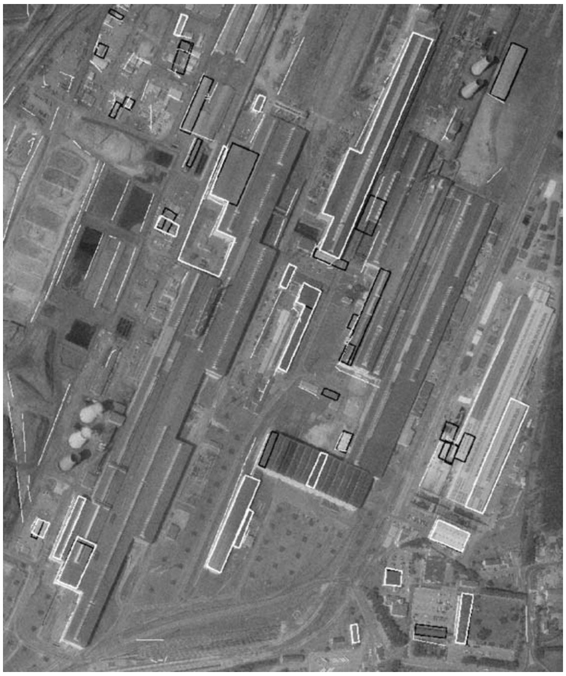

Fig. 11. Result of the automatic building detection: black and white polygons show objects detected by the rectangular box approach and the corner search tree, respectively, and white lines show SAR primitives.

The quantitative analysis of the results is difficult, since there are many small buildings in the concerned area. Therefore, we made the analysis relatively to the SAR primitives. The total number of SAR lines is 70. The number of false alarms for this parameter set is 10 (a building is wrongly detected or the given shape does not correspond to the true shape). It corresponds to a false alarm rate of 14%. There are 40 SAR primitives corresponding to building parts. Twenty-two buildings are well detected, 8 shapes correspond to building parts delimited by the roof and thus could be used for height filtering and 10 buildings are either not detected (too weak score) or detected with a wrong shape. The detection rate of the second step of the method is thus 55% and, if we include partial detection, 75%.

In a more qualitative way, the following comments can be made:

- The big building detection is difficult for many reasons. First, the SAR primitives are disconnected and correspond to a small part of the building. Besides, the method based on the corner search tree has the following limitations: the limited depth of the tree (due to combinatorial explosion); the weak contrast of some building corners which are therefore not detected (threshold thc_2); the limited size of the search area (s_g, although quite large); the presence of roof structures which leads to partial detections.
- The detection of middle and specially small buildings is rather satisfying since they often have a simple shape. Both methods give similar results except in the case of more complex shapes, but the rectangular box method is also less restrictive on the extremity detection. In both cases, the only criteria which are taken into account are the edge detector responses without verification of the region homogeneity. For both methods, the surrounding edges can lead to a wrong candidate.

7. Conclusion and further work

A first attempt to the simultaneous use of SAR and optical images for building detection has been presented. The proposed approach exploits the specific properties of each sensor, one giving the potential localization of the building and the other one permitting the search of the shape in this focusing area.

Many points could be improved. First, the SAR image could be used to validate the buildings detected in the optical image. Indeed, knowing the viewing direction and the building shape, the bright lines presence could be predicted and used as validation. Secondly, another approach for large buildings should be developed. For instance, the fusion score using the minimum operator could be relaxed to allow the detection of partial buildings, which could be merged at the end. Thirdly, the primitive SAR detection could be improved, for instance using a weaker threshold and a validation with the optical image.

References

Bloch, I., 1996. Information combination operators for data fusion: a comparative review with classification. IEEE Transactions on Systems, Man and Cybernetics SMC 26 (1), 52–67.

Bolter, R., Leberl, F., 2000. Detection and reconstruction of human scale features from high resolution interferometric SAR data. Proc. International Conference on Pattern Recognition, vol. 4, pp. 4291–4294.

Canny, J., 1986. A computational approach to edge detection. IEEE Transactions on Pattern Analysis and Machine Intelligence PAMI 8 (6), 679–698.

Deutsch, E.S., 1972. Thinning algorithms on rectangular, hexagonal, and triangular arrays. CACM 15 (9), 827–837.

Fatone, L., Maponi, P., Zirilli, F., 2001. Fusion of SAR/optical images to detect urban areas. Proc. IEEE/ISPRS Joint Workshop Remote Sensing and Data Fusion Over Urban Areas, pp. 217–221.

Gamba, P., Houshmand, B., Saccani, M., 2000. Detection and extraction of buildings from interferometric SAR data. IEEE Transactions on Geoscience and Remote Sensing 38 (1), 611–618.

Hanson, A., Jaynes, C., Riseman, E., Schultz, H., 1997. Building reconstruction from optical and range images. Proceedings on Computer Vision and Pattern Recognition, 380–386.

Hellwich, O., Günzl, M., Wiedemann, C., 2000. Fusion of optical imagery and SAR/INSAR data for object extraction. International Archives of Photogrammetry and Remote Sensing XXXIII (Part B3/1), 389–396.

Jaynes, C., Stolle, F., Collins, R., 1994. Task driven perceptual organization for extraction of rooftop polygons. Proc. ARPA Image Understanding Workshop, vol. 1, pp. 359–365.

Jordan, R., 1997. Shuttle radar topography mission system functional requirements document. Tech. Rep., JPL D-14293.

Lin, C., Huertas, A., Nevatia, R., 1995. Detection of buildings from monocular images. In: Gruen, A., Kuebler, O., Agouris, P. (Eds.), Automatic Extraction of Man-Made Objects from Aerial and Space Images. Birkhauser, Basel, pp. 125–134.

Oriot, H., Michel, A., Goretta, O., 1998. Extraction of rectangular roofs on stereoscopic images. An interactive approach. International Archives of Photogrammetry and Remote Sensing XXXII (Part 3), 367–373.

Roux, M., McKeown, D., 1994. Feature matching for building extraction from multiple views. Proc. IEEE Conference on Computer Vision and Pattern Recognition, Seattle, WA, pp. 46–53.

Shufelt, J.A., 1999. Performance evaluation and analysis of monocular building extraction from aerial imagery. IEEE Transactions on Pattern Analysis and Machine Vision 21 (4), 311–326.

Shufelt, J.A., McKeown, D.M., 1993. Fusion of monocular cues to detect man-made structures in aerial imagery. Computer Vision, Graphics and Image Processing-Image Understanding 57 (3), 307–330.

Simonetto, E., Oriot, H., Garello, R., 2000. Potentiality of high-resolution SAR images for radargrammetric applications. In: ESA SP-450, Harris, R.A., Ouwehand, L. (Eds.), Proc. CEOS Working Group Workshop on SAR Calibration and Validation, Toulouse, France, 26–29 October 1999. Available at http://www.estec.esa.nl/ceos99/papers/p160.pdf (accessed 29 January 2003).

Simonetto, E., Oriot, H., Garello, R., 2001. Extraction of industrial buildings from stereoscopic airborne radar images. Proc. 8th International Symposium on Remote Sensing, Toulouse, France, pp. 129–134.

Touzi, R., Lopes, A., Bousquet, P., 1988. A statistical and geometrical edge detector for SAR images. IEEE Transactions on Geoscience and Remote Sensing 26 (6), 764–773.

Tupin, F., 2002. Développement d'une approche figurale pour la radargrammétrie haute résolution en zone urbaine. Bulletin de la SFPT 166, 64–71.

Tupin, F., Maître, H., Mangin, J.-F., Nicolas, J.-M., Pechersky, E., 1998. Detection of linear features in SAR images: application to road network extraction. IEEE Transactions on Geoscience and Remote Sensing 36 (2), 434–453.

Xiao, R., Lesher, C., Wilson, B., 1998a. Building detection and localization using a fusion of interferometric synthetic aperture radar and multispectral image. Proc. ARPA Image Understanding Workshop, pp. 583–588.

Xiao, R., Wilson, R., Carande, R., 1998b. Neural network classification with IFSAR and multispectral data fusion. Proc. IGARSS, vol. 3, pp. 1327–1329.